Entropically Stabilized Local Dipole Formation in Lead Chalcogenides

Emil S. Božin,[1] Christos D. Malliakas,[2] Petros Souvatzis,[3] Thomas Proffen,[4] Nicola A. Spaldin,[5] Mercouri G. Kanatzidis,[2,6] Simon J. L. Billinge[1,7]*

We report the observation of local structural dipoles that emerge from an undistorted ground state on warming, in contrast to conventional structural phase transitions in which distortions emerge on cooling. Using experimental and theoretical probes of the local structure, we demonstrate this behavior in binary lead chalcogenides, which were believed to adopt the ideal, undistorted rock-salt structure at all temperatures. The behavior is consistent with a simple thermodynamic model in which the emerging dipoles are stabilized in the disordered state at high temperature due to the extra configurational entropy despite the fact that the undistorted structure has lower internal energy. Our findings shed light on the anomalous electronic and thermoelectric properties of the lead chalcogenides. Similar searches may show that the phenomenon is more widespread.

Ferroelectric materials are characterized by a spontaneous alignment of static local dipole moments leading to a net electric polarization that can be switched by an applied electric field (*1*). Above their critical Curie temperature, T_c, they undergo a phase transition to a higher symmetry, nonpolar state, which by analogy with ferromagnets is called paraelectric. Although the question of whether the paraelectric phase consists of fluctuating local dipole moments or entirely centrosymmetric arrangements of atoms remains open (and likely depends on material, temperature, and length scale), the transition from paraelectric to ferroelectric on cooling always involves a lowering in symmetry that is well described within the traditional Landau picture of phase transitions, for example, in $BaTiO_3$ (*2*). In PbTe and PbS, we have observed the existence at high temperature of such a paraelectric phase of disordered, fluctuating dipoles, but the ground state rather than being the ferroelectric state is a dielectric with no local dipoles. There is no macroscopic symmetry change associated with the spontaneous local dipole formation, so the behavior is invisible to conventional crystallographic techniques. We detect the local atomic off-centering at high temperature using recently developed local structural probes.

Lead chalcogenides such as PbTe and the mineral galena (PbS) have been known and exploited since ancient times (*3*). They are particularly important today, with PbTe currently the leading thermoelectric material in applications just above room temperature (*4*). Despite their long history, their nanoscale structure has only recently been studied in detail (*5*–*7*), motivated by the realization that intrinsic nanoscale structural modulations are helpful in producing low thermal conductivity and, therefore, high thermoelectric figures of merit (*4*, *8*). Such studies of the nanostructure have been enabled by powerful synchrotron-based local structure probes, such as atomic pair distribution function (PDF) analysis (*9*, *10*). The PDF is obtained by Fourier transforming appropriately collected and corrected x-ray or neutron powder diffraction data (*9*) and has peaks at positions corresponding to interatomic distances in the solid. We show in Fig. 1B the PDF of the simple rock-salt structure (Fig. 1A) that the lead chalcogenides were previously believed to adopt at all temperatures. Because both Bragg and diffuse scattering signals are used, the PDF yields local structural information rather than just the average crystallographic structure.

Our main results, obtained from temperature-dependent neutron diffraction studies, are summarized in Fig. 1, C to I. Because PbTe and PbS behave qualitatively similarly, we present only the PbTe results in the figure; data for PbS are contained in figs. S1 and S2 in the supporting online material (*11*). The dramatic effect of temperature on the structure of PbTe is evident in the powder diffraction pattern, shown in the form of the corrected and normalized diffraction intensity function $F(Q)$ (*11*) in Fig. 1C. This figure also serves to illustrate the high quality and good statistics of the neutron powder diffraction data collected over a wide range of momentum transfer, Q ($Q = 4\pi\sin\theta/\lambda$, where θ is the Bragg angle and λ the wavelength of the x-rays or neutrons). The dramatic loss of intensity in the Bragg peaks at high Q in the 500 K data (red) compared with the 15 K data (blue) is clear. The attenuation is due in part to the usual Debye-Waller effects (*12*) from increased thermal motion; however, the extent of the changes is extraordinarily large. In Fig. 1, D and E, we show the PDFs at 15 K and 500 K, respectively; the effect of temperature on the PDFs is anomalous, with notable broadening evident at 500 K compared with 15 K. (The scale in Fig. 1E is one-fifth that in Fig. 1D.)

To study the temperature-induced local structural effects in more detail, we next analyze the temperature dependence of the low-r region, where r is the interatomic pair separation distance, of the PDF (Fig. 1F), where measured PDFs are shown every 50 K from 15 K to 500 K. The PDF peak broadening is reflected in the drop in the maxima of the peaks. Particularly striking is the drop in the nearest-neighbor peak, which occurs as rapidly as those in the higher-neighbor peaks. This strong broadening of the nearest-neighbor PDF peak does not occur in conventional materials. This is because of the highly correlated dynamics of nearest-neighbor atoms (*13*), which results in the relative motion of directly bonded atom pairs having a much smaller temperature dependence than the higher-neighbor pairs.

In Fig. 1, G and H, we show the Pb-Te nearest-neighbor peak on an expanded scale. At 15 K (Fig. 1G), the peak appears as a sharp, single-Gaussian function with small ripples coming from the finite Q range of the Fourier transform, so-called termination ripples (*9*). The red line is a calculated PDF peak with a pure Gaussian line-shape, convoluted with a sinc function to simulate the effects of the finite Fourier transform (*9*). This is characteristic of a single average bond length with harmonic motion taking place around that position, indicating that the ground state of PbTe at 15K is ideal rock-salt in both the local and average structures, as expected. However, at 500 K (Fig. 1H), the peak is considerably broadened and qualitatively non-Gaussian, with extra intensity apparent on the high-r side of the peak. This unambiguously indicates the appearance of nonharmonic effects with increasing temperature.

We have quantified the asymmetry of this peak, and in Fig. 1I we plot the temperature dependence of a PDF peak asymmetry parameter, ΔR_{ASYMM} (*11*). It has a value of zero for a perfectly symmetric peak such as a Gaussian, and its numerical value increases as the peak becomes more asymmetric. As evident in Fig. 1I, the asymmetric nature of the first PDF peak increases continuously from 15 K to ~250 K, where it saturates.

The non-Gaussian asymmetry can be interpreted either in terms of strong anharmonicity in a single-welled potential probed by the atomic motions or by the appearance of multiple, incompletely resolved, short and long bond lengths under the nearest-neighbor PDF peak, characteristic of quasistatic structural dipoles in materials studied using the PDF (*14*, *15*). Figure 1F points to the latter interpretation because it is evident that higher-neighbor peaks are also losing their Gaussian character at high temperature. Despite being globally rock-salt, characteristic of lone-pair–inactive Pb^{2+} compounds (*6*), the local structure behaves like that in ferroelectrically distorted lone-pair–active Pb^{2+} compounds such as $PbTiO_3$ (*14*). The off-centered ions are disordered

[1]Condensed Matter Physics and Materials Science Department, Brookhaven National Laboratory, Upton, NY 11973, USA. [2]Department of Chemistry, Northwestern University, Evanston, IL 60208, USA. [3]Theoretical Division, Los Alamos National Laboratory, Los Alamos, NM 87545, USA. [4]Lujan Neutron Scattering Center, Los Alamos National Laboratory, Los Alamos, NM 87545, USA. [5]Department of Materials, ETH, Zurich, Switzerland. [6]Materials Science Division, Argonne National Laboratory, Argonne, IL 60439, USA. [7]Department of Applied Physics and Applied Mathematics, Columbia University, New York, NY 10027, USA.

*To whom correspondence should be addressed. E-mail: sb2896@columbia.edu

Report Documentation Page

Form Approved
OMB No. 0704-0188

1. REPORT DATE	2. REPORT TYPE	3. DATES COVERED
DEC 2010		**00-00-2010 to 00-00-2010**

4. TITLE AND SUBTITLE	5a. CONTRACT NUMBER
Entropically Stabilized Local Dipole Formation in Lead Chalcogenides	5b. GRANT NUMBER
	5c. PROGRAM ELEMENT NUMBER
6. AUTHOR(S)	5d. PROJECT NUMBER
	5e. TASK NUMBER
	5f. WORK UNIT NUMBER
7. PERFORMING ORGANIZATION NAME(S) AND ADDRESS(ES) **Brookhaven National Laboratory,Condensed Matter Physics and Materials Science Department,Upton,NY,11973**	8. PERFORMING ORGANIZATION REPORT NUMBER
9. SPONSORING/MONITORING AGENCY NAME(S) AND ADDRESS(ES)	10. SPONSOR/MONITOR'S ACRONYM(S)
	11. SPONSOR/MONITOR'S REPORT NUMBER(S)

12. DISTRIBUTION/AVAILABILITY STATEMENT
Approved for public release; distribution unlimited

13. SUPPLEMENTARY NOTES

14. ABSTRACT

15. SUBJECT TERMS

16. SECURITY CLASSIFICATION OF:			17. LIMITATION OF ABSTRACT	18. NUMBER OF PAGES	19a. NAME OF RESPONSIBLE PERSON
a. REPORT **unclassified**	b. ABSTRACT **unclassified**	c. THIS PAGE **unclassified**	**Same as Report (SAR)**	**4**	

among symmetry-equivalent displaced sites similar to the Ti in the high-temperature phases of $BaTiO_3$ (*14*). Although the PDF does not yield information directly on the dynamics, it is likely that the local dipole moments are fluctuating between the symmetry equivalent displaced sites.

Further confirmation of this unexpected result has been obtained by modeling the PDF using a least-squares fitting procedure (*11*). In Fig. 2A, the reduced χ^2 (goodness of fit) values of a number of competing models are shown as a function of temperature. Undistorted models give the best agreement at low temperature, but above 100 K distorted models give better agreement, with a model including displacements along ⟨100⟩ crystallographic directions being clearly preferred.

In Fig. 2, B and C, we show the T dependence of Pb isotropic atomic displacement parameters (ADPs) and the lattice parameter, respectively, refined from the simplest undistorted model. In this model, any off-centering must be accommodated in the refined ADP. The temperature dependence of both lattice parameters and the ADPs are linear, as expected, in the high-temperature region. In contrast, both properties show a downward deviation from this linear behavior below room temperature, precisely in the region where the PDF peak asymmetry is changing. This cannot be explained in any harmonic or quasiharmonic model for the lattice dynamics, such as the Debye model (*16*), shown as solid lines in the figure. The combined temperature dependences of the PDF peak asymmetry and the ADPs suggest that local ferroelectric-like Pb^{2+} off-center displacements, absent at T = 0 K, gradually emerge over the temperature range up to 250 K. At higher temperatures, the displaced ions show more conventional dynamics, resulting in a linear ADP and lattice expansion. The amplitude of the Pb^{2+} ion off-centering distortion, refined in the favored ⟨100⟩-displacements model, is shown in Fig. 2E. The refined distortion saturates at a maximum value of 0.24 Å. This is comparable in magnitude to ferroelectric displacements in, for example, $BaTiO_3$ (*2*). The vicinity of a ferroelectric instability is also implicated in first-principles electronic structure calculations (*7*), including our recently developed self-consistent ab initio lattice dynamical (SCAILD) method (*17*), as evident in fig. S3 (*11*).

Although the behavior observed in the PDF is highly unusual—we know of no other observation of local dipoles emerging from an undistorted ground state on heating—we rationalize it using a simple thermodynamic argument. In Fig. 3A, we plot the familiar schematic of the thermodynamic free energy, F, versus temperature for a series of phases.

The curves slope downward with increasing temperature, T, due to the increased contribution of the entropy term in the free energy at higher temperature: $F = U - TS$, where U is the internal energy. Phases with higher entropies, S, slope down more steeply and may cross below phases, with lower internal energy becoming the stable phase at high temperature. This is the classic explanation of the solid-liquid phase transition. In Fig. 3A, we represent the free energy of an ordered ferroelectric phase as a light blue line and that of the disordered paraelectric phase in olive green. In the absence of competing phases, the ferroelectric phase transition occurs at T_F, where these lines cross as indicated in the figure. Above T_F, the stable state is the paraelectric phase.

Another metastable state may exist that is undistorted but has a higher internal energy than the distorted phase. This is represented as a dashed gray line in Fig. 3B. Its configurational entropy should be the same as the ordered ferroelectric phase (light blue curve), so in the schematic we give these a similar slope, although factors such as vibrational entropy differences will change this somewhat in practice. Because it is higher in energy and has a similar slope, the free energy of this phase never crosses the ferroelectric phase, and it is never the stable state. However, consider the special situation in which this competing undistorted state is very close but slightly lower in energy than the ferroelectric state at T = 0. This situation is depicted as the red line in the figure. In this case,

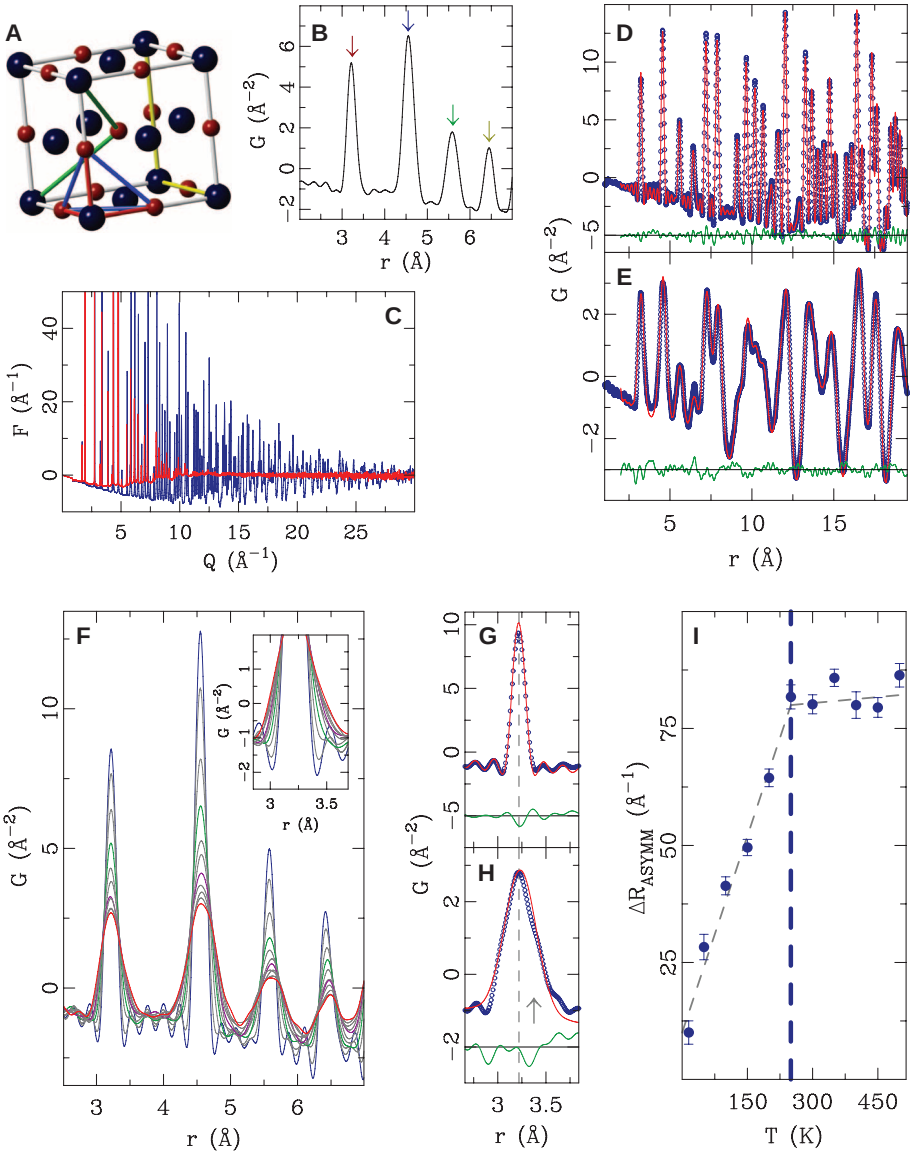

Fig. 1. (**A**) The rock-salt structure of PbTe with various interatomic distances color coded and (**B**) the respective PDF peaks marked with arrows using the same color code to illustrate how the PDF is built up from atom-pair distances in the structure. (**C**) Experimental total scattering structure function $F(Q)$ at T = 15 K (blue) and T = 500 K (red), with the corresponding PDFs (open symbols) shown in (**D**) and (**E**). The PDF of the rock-salt structure model is superimposed as a solid red line, with the difference curve (green) offset for clarity. (**F**) A stack of experimental PDFs from 15 K (blue) to 500 K (red) in ~50 K increments. The 150 K data set is highlighted in green, and the 300 K data are in purple. The inset focuses on the behavior of the nearest-neighbor PDF peak. (**G**) Fit of the rock-salt crystallographic model to the near-neighbor PDF peak data at 15 K and (**H**) at 500 K. (**I**) Asymmetry of the near-neighbor PDF peak.

the ground state is undistorted, but on warming the stable state becomes the paraelectric phase, and local fluctuating dipoles emerge out of an undistorted ground state. This crossover is indicated by T_E in the figure. These thermodynamic arguments do not explain the phenomenon, but they give an intuitive rationalization for this behavior and suggest that it may be more widespread than in the PbQ compounds studied here.

The thermodynamic arguments do not address the microscopic mechanisms that could give rise to this situation, nor do they address the precise nature of the transition from the undistorted to the paraelectric phase, that is, whether it is an abrupt transition or a diffuse crossover. The short-range nature of the dipole fluctuations suggests the latter, although characterizing this will require further study. Although there is no change in crystal symmetry, so it is not possible to identify a macroscopic order parameter, there is evidence for the transition in a macroscopic structural parameter: An anomaly is evident in the temperature dependence of the lattice parameter (Fig. 2B), which shows a similar negative deviation from linear behavior at 250 K.

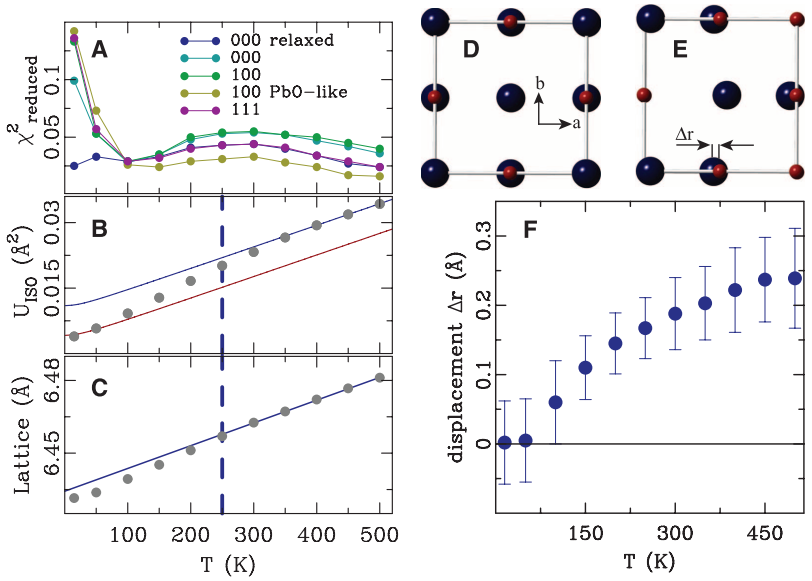

Fig. 2. (**A**) Reduced χ^2 of best fits for competing models of the local structure (*11*). (**B**) The gray dots are the isotropic ADPs for Pb refined from the undistorted model. The solid lines represent the behavior expected from the Debye model, using the same Debye temperature, but with different offset parameters, accounting for static disorder, for the red and blue lines. (**C**) The PbTe lattice parameter (gray dots) as obtained from Rietveld refinement. The vertical dashed line indicates the temperature 250 K where the asymmetry of the nearest-neighbor peak saturates (Fig. 1I). (**D**) Schematic of the rock-salt structure shown in projection down the *c* axis, showing Pb (blue) and Te (red). (**E**) Same view of the proposed model for the distorted rock-salt structure above room temperature. The amplitude of the Pb displacements have been highly exaggerated to show the displacements more clearly. (**F**) Amplitude of Pb local off-centering refined from the ⟨100⟩ displaced model.

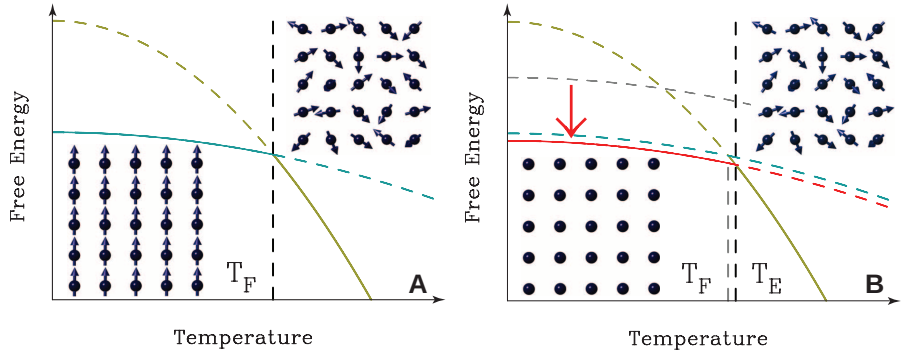

Fig. 3. Schematics of the temperature dependence of the thermodynamic free energy *F*. (**A**) The light blue curve represents *F*(*T*) for a ferroelectric state with ordered dipole moments (shown schematically as blue arrows), and the olive green curve is for the paraelectric state where the dipoles are fluctuating and only short-range ordered at best. It is more steeply sloping because of the extra configurational entropy. Where these curves cross is the ferroelectric transition temperature, labeled T_F. The blue arrows show schematically the ordered dipole moments in the ferroelectric phase and disordered moments in the paraelectric phase. (**B**) As in (A) but superimposed are additional free-energy curves for putative undistorted states. The gray dashed curve represents *F*(*T*) for a metastable undistorted state. The red curve shows the case where the competing undistorted state is slightly lower in energy than the ferroelectric state. In this case, there is a crossover from an undistorted to a paraelectric phase at a temperature T_E, as shown schematically. In the insets, the blue dots indicate the absence of dipoles at low temperature and the blue arrows the disordered fluctuating dipoles at high temperature.

The structural effects we report should be considered in future explanations of the peculiar properties of these materials; for example, the very low lattice thermal conductivity (*18*) at elevated temperatures. The ferroelectric-like moment fluctuations would also explain the well-known strong temperature dependence of carrier scattering, which is unique in PbQ and not found in other semiconductors such as Si, Ge, and Bi_2Te_3. This dependence causes the rapid degradation of carrier mobility with rising temperature with a $T^{-2.5}$ dependence (*19*). Generally, the power exponent for the mobility in semiconductors is $\sim T^{-1.5}$, and it is due to the increase in vibrational amplitude of the lattice. The high power exponent in PbQ implies additional scattering mechanisms for the carriers that would come from the local off-centering fluctuations of the Pb^{2+} ions. Similarly, our electronic structure calculations (*11*) find an enhanced band gap for the locally distorted structure, indicating that the observed anomalous increase in the band gap, E_g, with increasing temperature observed in PbTe (*20*), may be explained by the appearance of the local distortions.

The emergence of structural dipoles from normal, undistorted states in materials may be more ubiquitous than currently recognized. There are some similarities of the present situation to the search for a hidden broken symmetry in the pseudogap phase of high-temperature superconductors, where a short-range nematic orbital ordering may be relevant but is only apparent in probes of local structure (*21*). The PDF is a powerful experimental tool for probing these effects. Finally, we may now begin to contemplate new ways to control these fluctuations through appropriate chemical modifications that could lead to large increases in the thermoelectric performance of PbTe-based materials. We suggest in particular that new thermoelectrics should be sought among materials that, like PbTe, are close to a ferroelectric instability. It is remarkable that binary compounds with such simple structures, which have been known about and exploited for thousands of years, can still harbor surprises when studied using modern experimental and theoretical tools.

References and Notes

1. F. Jona, G. Shirane, *Ferroelectric Crystals* (Dover, New York, 1993).
2. G. H. Kwei, A. C. Lawson, S. J. L. Billinge, S.-W. Cheong, *J. Phys. Chem.* **97**, 2368 (1993).
3. P. Walter *et al.*, *Nano Lett.* **6**, 2215 (2006).

4. Z. H. Dughaish, *Physica B* **322**, 205 (2002).
5. H. Lin, E. S. Bozin, S. J. L. Billinge, E. Quarez, M. G. Kanatzidis, *Phys. Rev. B* **72**, 174113 (2005).
6. U. V. Waghmare, N. A. Spaldin, H. C. Kandpal, R. Seshadri, *Phys. Rev. B* **67**, 125111 (2003).
7. J. M. An, A. Subedi, D. J. Singh, *Solid State Commun.* **148**, 417 (2008).
8. J. R. Sootsman *et al.*, *Angew. Chem. Int. Ed.* **47**, 8618 (2008).
9. T. Egami, S. J. L. Billinge, *Underneath the Bragg Peaks: Structural Analysis of Complex Materials* (Pergamon Press, Elsevier, Oxford, England, 2003).
10. S. J. L. Billinge, I. Levin, *Science* **316**, 561 (2007).
11. Materials and methods are available as supporting material on *Science* Online.
12. B. E. Warren, *X-ray Diffraction* (Dover, New York, 1990).
13. I.-K. Jeong, T. Proffen, F. Mohiuddin-Jacobs, S. J. L. Billinge, *J. Phys. Chem. A* **103**, 921 (1999).
14. G. H. Kwei, S. J. L. Billinge, S.-W. Cheong, J. G. Saxton, *Ferroelectrics* **164**, 57 (1995).
15. H. D. Rosenfeld, T. Egami, *Ferroelectrics* **164**, 133 (1995).
16. P. Debye, *Ann. Phys.-Berlin* **39**, 789 (1912).
17. P. Souvatzis, O. Eriksson, M. I. Katsnelson, S. P. Rudin, *Phys. Rev. Lett.* **100**, 095901 (2008).
18. A. F. Joffé, *Can. J. Phys.* **34**, (12A), 1342 (1956).
19. B. A. E. Yu, I. Ravich, I. A. Smirnov, *Semiconducting Lead Chalcogenides*, vol. 5 (Plenum, New York, 1970).
20. R. N. Tauber, A. A. Machonis, I. B. Cadoff, *J. Appl. Phys.* **37**, 4855 (1966).
21. T. M. Chuang *et al.*, *Science* **327**, 181 (2010).
22. S.J.B. and E.B. thank J. Richardson for his early support and enthusiasm for the project and dedicate the paper to him. We acknowledge useful discussions with A. Millis, P. Allen, R. Cohen, C. Farrow, and J. Hill. Work in the Billinge group was supported by the U.S. Department of Energy, Office of Basic Energy Sciences (DOE-BES), under contract DE-AC02-98CH10886. Work in the Kanatzidis group was supported by the Office of Naval Research. Work in the Spaldin group was supported by the NSF under award DMR-0940420. The neutron diffraction measurements were carried out at the Lujan Center at Los Alamos National Laboratory, and the x-ray experiments were carried out at the Advanced Photon Source, Argonne National Laboratory, both of which are supported by DOE-BES, and the calculations were performed at the San Diego Supercomputer Center, which is supported by NSF.

Supporting Online Material

www.sciencemag.org/cgi/content/full/330/6011/1660/DC1
Materials and Methods
SOM Text
Figs. S1 to S4
References

24 May 2010; accepted 16 November 2010
10.1126/science.1192759

Large Variations in Southern Hemisphere Biomass Burning During the Last 650 Years

Z. Wang,[1] J. Chappellaz,[2] K. Park,[1] J. E. Mak[1]*

We present a 650-year Antarctic ice core record of concentration and isotopic ratios ($\delta^{13}C$ and $\delta^{18}O$) of atmospheric carbon monoxide. Concentrations decreased by ~25% (14 parts per billion by volume) from the mid-1300s to the 1600s then recovered completely by the late 1800s. $\delta^{13}C$ and $\delta^{18}O$ decreased by about 2 and 4 per mil (‰), respectively, from the mid-1300s to the 1600s then increased by about 2.5 and 4‰ by the late 1800s. These observations and isotope mass balance model results imply that large variations in the degree of biomass burning in the Southern Hemisphere occurred during the last 650 years, with a decrease by about 50% in the 1600s, an increase of about 100% by the late 1800s, and another decrease by about 70% from the late 1800s to present day.

Carbon monoxide (CO) plays a key role in the chemistry of the troposphere, largely determining the oxidation potential of the atmosphere through its interaction with hydroxyl radical (OH). CO also interacts with atmospheric methane, a gas whose preindustrial variability is the topic of continuing debate (*1*, *2*). Little is known about the variability of CO before the industrial age (*3*) or about the anthropogenic impact on its budget, although both affect atmospheric CH_4 and O_3 budgets and related climate-chemistry interactions.

The main sources of atmospheric CO include atmospheric oxidation of methane and nonmethane hydrocarbons (NMHCs), biomass burning, and fossil fuel combustion (*4*). These sources account for about 90% of today's global CO budget (*4*). Stable isotopic ratios ($\delta^{13}C$ and $\delta^{18}O$) in atmospheric CO help to resolve the relative contributions of these sources and thus to better estimate the global CO budget (*5*). To date, no isotopic ratios from CO in ice have been reported, and few CO mixing ratio measurements have been reported (*1*, *3*, *6*). Through use of a recently developed analytical technique (*7*), we present measurements of CO concentration ([CO]), $\delta^{13}C$, and $\delta^{18}O$ from a South Pole ice core [89°57'S 17°36'W; 2800 m above sea level (asl)] and from the D47 ice core (67°23'S 154°03'E; 1550 m asl) in Antarctica (Fig. 1).

The combined changes in [CO], $\delta^{13}C$, and $\delta^{18}O$ during the past 650 years should reflect variations in both total CO flux and a shift in relative source strengths over time. [CO] shows a decreasing trend from 53 ± 5 parts per billion by volume (ppbv) in the mid-1300s to a minimum of 38 ± 5 ppbv in the 1600s. CO mixing ratio then increases to a relatively constant value of 55 ± 5 ppbv in the late 1800s. Good agreement was observed between our [CO] data and previous measurements on Antarctic ice samples (*3*, *6*). Trends in both $\delta^{13}C$ and $\delta^{18}O$ look similar to the [CO] record up to the late 1800s. $\delta^{13}C$ [Vienna Pee Dee belemnite (VPDB)] and $\delta^{18}O$ [Vienna standard mean ocean water (VSMOW)], respectively, decreased from –28.0 ± 0.3‰ and 0.6 ± 0.7‰ in the mid-1300s to –30.2 ± 0.3‰ and –3.4 ± 0.7‰ in the 1600s, then increased to –27.4 ± 0.3‰ and 0.8 ± 0.7‰ by the late 1800s. Minimum values of [CO], $\delta^{13}C$, and $\delta^{18}O$ roughly coincide with the Little Ice Age (LIA; circa 1500–1800), as defined in the Northern Hemisphere.

Observations from Berkner Island (79°32.90'S 45°40.7'W; 890 m asl) firn and present day samples are also shown in Fig. 1. The slight decrease of [CO] from the late 1800s to present day is thus accompanied by large shifts in both $\delta^{13}C$ and $\delta^{18}O$, which is a result of variations in relative source strengths during the past century. In particular, methane-derived CO, which is dependent upon methane concentration and depleted in both $\delta^{13}C$ and $\delta^{18}O$, increased dramatically—by 13 ppbv—during this time (Fig. 2). Because there was little difference in overall [CO] between the late 1800s and present day, contributions from other CO sources must have decreased by a similar amount. Data from Berkner Island firn air show an increase in [CO] and a decrease in $\delta^{13}C$ since 1970 (*8*), reflecting the increase in atmospheric methane (*9*).

The contribution from fossil fuel combustion is negligible before the 1900s according to historic CO_2 emissions data (*10*). In addition, simulations from the Model for Ozone and Related chemical Tracers (MOZART-4) (*11*) show the fossil fuel combustion contribution to today's CO budget in Antarctica is only 2 to 3 ppbv. Thus, the main sources of CO able to explain our signals are biomass burning and NMHC oxidation.

We can use isotopic compositions to help distinguish combustion-derived CO (such as biomass burning) from noncombustion-derived CO (such as hydrocarbon oxidation). $C^{18}O$ is a useful tracer for this because of large differences in the oxygen isotopic composition between combustion and noncombustion sources of CO (*12*). The $\delta^{18}O$ signature from combustion sources is significantly enriched as compared with the $\delta^{18}O$ signature from hydrocarbon oxidation processes (*12*, *13*). The $\delta^{18}O$ value for biomass burning–derived CO is generally between 15 and 22‰, depending on specific combustion conditions (*13*–*15*).

We used an isotope mass balance model to estimate the ratio of combustion to noncombustion

[1]Institute for Terrestrial and Planetary Atmospheres/School of Marine and Atmospheric Sciences, Stony Brook University, Stony Brook, NY 11794–5000, USA. [2]Laboratoire de Glaciologie et Géophysique de l'Environnement (LGGE), CNRS, University of Grenoble, BP 96, 38402 St. Martin d'Hères Cedex, France.

*To whom correspondence should be addressed. E-mail: john.mak@stonybrook.edu